Effect of large displacements on the linearized vibration of composite beams

Effect of large displacements on the vibration response of composite beams

E. Carrera[*], A. Pagani[†], R. Augello[‡]

Mul^2 Group
Department of Mechanical and Aerospace Engineering, Politecnico di Torino
Corso Duca degli Abruzzi 24, 10129 Torino, Italy.

Abstract: *Natural frequencies and mode shapes are functions of the equilibrium state. In the large displacement regime, pre-stresses may modify significantly the modal behaviour of structures. In this work, a geometrical nonlinear total Lagrangian formulation that includes cross-sectional deformations is developed to analyse the vibration modes of composite beams structures in the nonlinear regime. Equations of motion are solved around nonlinear static equilibrium states, which are identified using a Newton-Raphson algorithm along with a path-following method of arc-length type. Different boundary conditions and stacking sequences are analysed. It is shown that vibration modes are strongly modified by nonlinear phenomena. Moreover, models that do not describe those effects accurately may results in misleading results, especially if compression is dominant. In fact, results show a crossing phenomenon in the post-buckling regime of an asymmetric cross-ply beam, whereas it is completely unforeseen by the linearized analysis.*

Keywords: Nonlinear vibration; Mode aberration; Composite beams; Geometrical nonlinear analysis; Carrera Unified Formulation.

1 Introduction

The design process and the verification of composite structures demand for accurate evaluation of their dynamic characteristics; i.e., natural frequencies and mode shapes. Since the modal behaviour of a structure is strictly related to the equilibrium condition and the pre-stresses, the dynamic characteristics can change as the equilibrium state changes, which is particularly true in the case of large displacements and rotations when the equilibrium is far from the trivial state.

The static and dynamic properties of a body undergoing considerable pre-stress conditions were analyzed by Biot [1], who developed a nonlinear theory, including first and second order terms to describe the kinematic relations. Abkarov [2] offered a review of analyses carried out on the evaluation of the dynamic properties of bodies with initial stresses. For example, Akbarov and Ozisik [3] conducted a study on the dynamic properties of a pre-stressed nonlinear layer. The influence of initial stress on dynamic characteristics was also

[*]Professor of Aerospace Structures and Aeroelasticity
[†]Assistant Professor. Corresponding author. E-mail: alfonso.pagani@polito.it
[‡]Post Graduate Research Assistant. E-mail: riccardo.augello@polito.it

studied for elastic plates, for both isotropic (see Ogden and Roxburgh [4] and Herrmann [5]) and composite structures (see Sun and Whitney [6]).

Vibration of structures is a topic widely investigated by researcher and scientists. To evaluate the dynamic properties of composite structures, many authors analyzed the free vibration characteristics for their studies. The work made by Virgin [7] presented a deep analysis of the vibration properties of slender structures subjected to compressive loadings. Moreover, based on Timoshenko beam theory [8], Ke *et al.* [9] analyzed the dynamic characteristic of functionally graded nanocomposite beams using von Kármán geometrical nonlinear approximation, while Zhu *et al.* [10] conducted comparable analyses in the case of carbon nanotube reinforced composite plates. Leissa [11, 12] and Leissa and Qatu [13] proposed a description of classical plate and shell theories, considering different geometrical and material characteristics. Regarding composite beams, Hodges *et al.* [14] showed methods for the evaluation of the natural frequencies and the associated modal shapes, using the Finite Element Method (FEM) to solve the equations of motion. Moreover, free vibrations of composite beams were investigated by Chandrashekhara *et al.* [15], considering rotary inertia and first-order shear deformations, and by Chandrashekhara and Bangera [16], using a refined higher-order shear deformation theory. Both works showed the effect of geometric and material properties and boundary conditions on dynamic properties of composite beams. Moreover, Song and Librescu [17] analyzed the free vibration of anisotropic beams with thick - and thin-walled cross-sections, whereas Lee [18] studied delaminated composite beams, adopting a layerwise approach. Regarding plates, Kant and Swaminathan [19] used a higher-order theory to develope a refined model for the free vibration analysis of laminated sandwich plates. Besides, simply-supported multilayered composite plates were studied by Noor and Burton [20].

During the last years, composite structures have been largely adopted in many engineering applications, from the automotive to the aerospace fields. For this reason, scientists and researchers were led to develop ad-hoc mathematical models to describe the mechanical behaviour of composite structures. A comprehensive review about the modeling of composite laminates for one- and two-dimensional structures can be found in Kapania and Raciti [21, 22] and Zhang and Yang [23]. As an example, Reddy [24] proposed a two-dimensional shear deformation theory of composite plates. The works by Hodges [25] and Chia [26] presented an overview of the geometrically nonlinear behaviour of composite beams and plates, respectively. The literature of works about the behaviour of composite structures in the large displacement and rotation field is vast, indeed. As an example, the work by Zhang and Kim [27] is mentioned, which proposes a quadrilateral plate element for the geometrical nonlinear analysis of laminated composite plate. The model is based on first-order shear deformation theory and von Kármán geometrical nonlinearity, with a total Lagrangian approach. With the same assumptions, Zhang and Liew [28] analyzed the geometrical nonlinear behaviour of carbon nanotube reinforced composite plates.

The present work intends to investigate the change of natural frequency and associated mode shapes in the case of large displacements/rotations of composite beam structures. A similar approach can be found in a real application, see Abramovich *et al.* [29] and Arbelo *et al.* [30], who developed a not-destructive method for the evaluation of critical buckling load of metallic structure, by interpolating until singularity the natural frequencies calculated experimentally at progressive loadings. The proposed nonlinear model was developed in the framework of the Carrera Unified Formulation (CUF) [31, 32]. According to CUF, any theory of structures can be expressed as a generic expansion of the primary unknowns. In this manner, the order of the theory is considered as input of the analysis, so that the generation of low- to high-order finite beam elements is possible. The nonlinear governing equations are

written, in fact, in terms of *fundamental nuclei*, that can be opportunely expanded according to the order of the theory. Over the last few years, CUF has been expanded to deal with various engineering problems, such as micromechanics [33], civil engineering structures [34], nonlinear problems [35, 36], hygrothermal analysis [37] and multi-field problems [38].

This paper is organized as follows: (i) first, CUF and the related finite element is briefly introduced in Section 2; (ii) subsequently, Section 3 shows the linearized eigenvalue problem solved along the geometrical nonlinear analysis to evaluate the mode change. The *fundamental nuclei* of both secant and tangent stiffness matrices are introduced next; (iii) then, Section 4 reports the obtained results, and those deal with a cantilever asymmetric beam subjected to bending uniform pressure, the post-buckling of a simply-supported symmetric beam and a cantilever asymmetric beam undergoing a compressive load with three different stacking sequences considered; (iv) finally, the main conclusions are reported in Section 5.

2 Higher-order one-dimensional element

Let us suppose a one-dimensional (1D) structure, with the cross-section laying on the xz-plane of a Cartesian reference system. Then, y represents the direction of the beam axis. The displacement vector is given by:

$$\mathbf{u}(x,y,z;t) = \left\{ \begin{array}{ccc} u_x & u_y & u_z \end{array} \right\}^T \tag{1}$$

The stress, $\boldsymbol{\sigma}$, and strain, $\boldsymbol{\epsilon}$, components are expressed in vectorial form with no loss of generality,

$$\boldsymbol{\sigma} = \left\{ \begin{array}{cccccc} \sigma_{xx} & \sigma_{yy} & \sigma_{zz} & \sigma_{xz} & \sigma_{yz} & \sigma_{xy} \end{array} \right\}^T, \quad \boldsymbol{\epsilon} = \left\{ \begin{array}{cccccc} \epsilon_{xx} & \epsilon_{yy} & \epsilon_{zz} & \epsilon_{xz} & \epsilon_{yz} & \epsilon_{xy} \end{array} \right\}^T \tag{2}$$

In this work, composite beam structures are considered. The constitutive relation takes the form:

$$\boldsymbol{\sigma} = \mathbf{C}\boldsymbol{\epsilon} \tag{3}$$

where $\mathbf{C}$ represents the material matrix, see [36]. Note that linear elastic materials are considered in this study. As far as the geometrical nonlinear relations are concerned, the Green-Lagrange strains are retained; they read

$$\boldsymbol{\epsilon} = \boldsymbol{\epsilon}_l + \boldsymbol{\epsilon}_{nl} = (\mathbf{b}_l + \mathbf{b}_{nl})\mathbf{u} \tag{4}$$

where $\mathbf{b}_l$ and $\mathbf{b}_{nl}$ are the linear and nonlinear differential operators, respectively. Interested readers may refer to [35, 39] for more details about $\mathbf{b}_l$ and $\mathbf{b}_{nl}$.
According to the Carrera Unified Formulation (CUF) (see Carrera *et al.* [32]), in the case of 1D structure, the three-dimensional displacement field $\mathbf{u}(x,y,z;t)$ can be expressed as:

$$\mathbf{u}(x,y,z;t) = F_s(x,z)\mathbf{u}_s(y;t), \qquad s = 1,2,....,M \tag{5}$$

where F_s are the expansion functions of the coordinates x and z on the cross-section, $\mathbf{u}_s$ is the vector of the displacements along the beam axis direction, M stands for the number of the terms used in the expansion, and the subscript s indicates summation. The proposed work adopts Lagrange polynomials as F_s to approximate the beam theory kinematics. In this manner, higher-order models with layerwise capabilities can be implemented with ease (see

the work by Carrera and Petrolo [40] for more details). As an example, the displacement field evaluated through one L9 polynomial is quadratic and reads:

$$\begin{aligned} u_x(x,y,z;t) &= F_1(x,z)u_{x_1}(y;t) + F_2(x,z)u_{x_2}(y;t) + ... + F_9(x,z)u_{x_9}(y;t) \\ u_y(x,y,z;t) &= F_1(x,z)u_{y_1}(y;t) + F_2(x,z)u_{y_2}(y;t) + ... + F_9(x,z)u_{y_9}(y;t) \\ u_z(x,y,z;t) &= F_1(x,z)u_{z_1}(y;t) + F_2(x,z)u_{z_2}(y;t) + ... + F_9(x,z)u_{z_9}(y;t) \end{aligned} \tag{6}$$

where $u_{x1}, \ldots, u_{z9}$ are the displacement of the points of the cross-sectional elements and F_1 to F_9 are functions of the cross-sectional coordinates and represent the first 9 Lagrange polynomials of order 3. Complex cross-section geometries and piece-wise higher-order kinematics can be developed by opportunely using a combination of Lagrange polynomials. More details about the Lagrange expansion are described in [41].
To approximate the displacement field over the beam axis, the Finite Element Method (FEM) is adopted. The generalized displacement vector $\mathbf{u}_s(y)$ is approximated as follows:

$$\mathbf{u}_s(y;t) = N_j(y)\mathbf{q}_{sj}(t) \qquad j = 1, 2, \ldots, p+1 \tag{7}$$

where N_j stands for the j-th shape function, p is the order of the shape functions and j indicates summation. $\mathbf{q}_{sj}$ is the following vector of the FE nodal parameters:

$$\mathbf{q}_{sj}(t) = \left\{ \begin{array}{ccc} q_{x_{sj}} & q_{y_{sj}} & q_{z_{sj}} \end{array} \right\}^T \tag{8}$$

For the sake of brevity, the shape functions N_j are not reported here. They can be found for instance in Bathe [42] and in Carrera *et al.* [32]. The proposed research work makes use of classical 1D finite Lagrangian elements with four nodes (B4) which provides a cubic interpolation along the y axis.

3 Linearized vibration modes of structures undergoing large displacements

Using the principle of virtual work, the equations of motion of a un-damped elastic body subjected to inertia forces and no external forces can be expressed as follows:

$$\delta L_{\text{int}} = -\delta L_{\text{ine}} \tag{9}$$

where L_{int} stands for the work of the internal forces, L_{ine} is the work made by the inertial loads, and δ denotes the virtual variation. Given the stress ($\boldsymbol{\sigma}$) and strain ($\boldsymbol{\epsilon}$) vectors as in Eq. (2), the virtual variation of the internal strain energy can be written as

$$\delta L_{\text{int}} = \int_V \left(\delta \boldsymbol{\epsilon}^T \boldsymbol{\sigma} \right) \, \mathrm{d}V \tag{10}$$

where V represents the body volume. Introducing CUF (Eq. (5)) and FEM (Eq. (7)) equations into Eq. (4), the strain vector reads, in algebraic form:

$$\boldsymbol{\epsilon} = \left(\mathbf{B}_l^{sj} + \mathbf{B}_{nl}^{sj} \right) \mathbf{q}_{sj} \tag{11}$$

where $\mathbf{B}_l^{sj}$ and $\mathbf{B}_{nl}^{sj}$ are linear and nonlinear algebraic matrices. Those matrices are not explicitely reported here for the sake of brevity, but they can be found in [36].
Introducing Eq. (11) and the constitutive relation (Eq. (3)) into Eq. (10), one has:

$$\begin{aligned}
\delta L_{\text{int}} &= \delta \mathbf{q}_{\tau i}^T \int_V \left((\mathbf{B}_l^{\tau i} + 2\,\mathbf{B}_{nl}^{\tau i})^T \mathbf{C} (\mathbf{B}_l^{sj} + \mathbf{B}_{nl}^{sj})\, \mathrm{d}V \right)\, \mathbf{q}_{sj} \\
&= \delta \mathbf{q}_{\tau i}^T \mathbf{K}_0^{ij\tau s}\, \mathbf{q}_{sj} + \delta \mathbf{q}_{\tau i}^T \mathbf{K}_{lnl}^{ij\tau s}\, \mathbf{q}_{sj} + \delta \mathbf{q}_{\tau i}^T \mathbf{K}_{nll}^{ij\tau s}\, \mathbf{q}_{sj} + \delta \mathbf{q}_{\tau i}^T \mathbf{K}_{nlnl}^{ij\tau s}\, \mathbf{q}_{sj} \\
&= \delta \mathbf{q}_{\tau i}^T \mathbf{K}_S^{ij\tau s}\, \mathbf{q}_{sj}
\end{aligned} \tag{12}$$

where $\mathbf{K}_S^{ij\tau s}$ is the secant stiffness matrix, $\mathbf{K}_0^{ij\tau s}$ is the linear contribution of the secant stiffness matrix and $\mathbf{K}_{lnl}^{ij\tau s}$, $\mathbf{K}_{nll}^{ij\tau s}$ and $\mathbf{K}_{nlnl}^{ij\tau s}$ are the nonlinear contributions. These contributions are written in the form of the so-called fundamental nuclei (FN). By opportunely choosing the index for the cross-sectional expansion functions and axial shape functions, FN can be arbitrarily expanded in order to reach any order of theory to model the structure. The explicit derivation of the stiffness FN can be found in [35].
The evaluation of the linearized free vibration modes around nonlinear equilibrium states (see Fig. 1) demands for the linearization of the equations of motion of Eq. (9). The linearized form of the Eq. (9) yelds:

$$\delta(\delta L_{\text{int}}) = -\delta(\delta L_{\text{ine}}) \tag{13}$$

As far as the linearization of the internal strain energy is concerned, it reads:

$$\begin{aligned}
\delta(\delta L_{\text{int}}) &= \int_V \delta \left(\delta \boldsymbol{\epsilon}^T \boldsymbol{\sigma} \right)\, \mathrm{d}V \\
&= \int_V \delta \boldsymbol{\epsilon}^T \delta \boldsymbol{\sigma}\, \mathrm{d}V + \int_V \delta \left(\delta \boldsymbol{\epsilon}^T \right) \boldsymbol{\sigma}\, \mathrm{d}V
\end{aligned} \tag{14}$$

where the first term in right-hand-side calls for the linearization of the constitutive relations, whereas the second term will involve the linerization of the geometrical relations. Introducing Eq. (11) into the Eq. (14), $\delta(\delta L_{\text{int}})$ takes the form:

$$\begin{aligned}
\delta(\delta L_{\text{int}}) &= \delta \mathbf{q}_{\tau i}^T \left(\mathbf{K}_0^{ij\tau s} + \mathbf{K}_{T_1}^{ij\tau s} \right) \delta \mathbf{q}_{sj} + \delta \mathbf{q}_{\tau i}^T \mathbf{K}_\sigma^{ij\tau s} \delta \mathbf{q}_{sj} \\
&= \delta \mathbf{q}_{\tau i}^T \mathbf{K}_T^{ij\tau s} \delta \mathbf{q}_{sj}
\end{aligned} \tag{15}$$

where $\mathbf{K}_T^{ij\tau s}$ represent the FN of the tangent stiffness matrix. Note that $\mathbf{K}_T^{ij\tau s} = \mathbf{K}_0^{ij\tau s} + \mathbf{K}_{T_1}^{ij\tau s} + \mathbf{K}_\sigma^{ij\tau s}$. $\mathbf{K}_0^{ij\tau s}$ is the linear contribution, $\mathbf{K}_{T_1}^{ij\tau s}$ equals to $2\mathbf{K}_{lnl}^{ij\tau s} + \mathbf{K}_{nll}^{ij\tau s} + 2\mathbf{K}_{nlnl}^{ij\tau s}$, and $\mathbf{K}_\sigma^{ij\tau s}$ represents the so-called geometric stiffness [43]. It takes into account both linear and nonlinear pre-stress states. The explicit form of the tangent stiffness matrix is given in [35]. In the next step - by using the aforementioned relations, assuming constant mass, neglecting higher-order

nonlinearities, and after opportune manipulations - the linearization of the virtual variation of the inertia loadings is expressed as follows:

$$\begin{aligned} \delta(\delta L_{\text{ine}}) &= \delta\left(\int_V \delta\mathbf{u}^T \boldsymbol{\rho}\, \ddot{\mathbf{u}}\, \mathrm{d}V\right) = \delta\left(\delta\mathbf{q}_{sj}^T \mathbf{M}^{ij\tau s}\, \ddot{\mathbf{q}}_{\tau i}\right) \\ &= \delta\mathbf{q}_{sj}^T \mathbf{M}^{ij\tau s}\, \delta\ddot{\mathbf{q}}_{\tau i} \end{aligned} \tag{16}$$

where $\mathbf{M}^{ij\tau s}$ is the FN of the elemental, linear mass matrix. Substituting Eqs. (15) and (16) into the Eq. (13), one has:

$$\delta\mathbf{q}_{\tau i}^T \mathbf{K}_T^{ij\tau s} \delta\mathbf{q}_{sj} = -\delta\mathbf{q}_{\tau i}^T \mathbf{M}^{ij\tau s}\, \delta\ddot{\mathbf{q}}_{sj} \tag{17}$$

Given the nature of the problem in hand and the hypothesis made, it is reasonable to assume harmonic motion around linearized states along the nonlinear equilibrium path. Thus, one has:

$$\begin{aligned} \delta\mathbf{q}_{sj}(t) &= \delta\bar{\mathbf{q}}_{sj}\, e^{i\omega t} \\ \delta\ddot{\mathbf{q}}_{\tau i}(t) &= -\omega^2\, \delta\bar{\mathbf{q}}_{sj}\, e^{i\omega t} \end{aligned} \tag{18}$$

Finally, substituting Eq. (18) into Eq. (17), the equations of motion take the form of a linear eigenvalue problem:

$$\left(\mathbf{K}_T^{ij\tau s} - \omega^2 \mathbf{M}^{ij\tau s}\right)\, \delta\bar{\mathbf{q}}_{sj} = \mathbf{0} \tag{19}$$

Note that:

- Given a structure and prescribed the boundary conditions, the quasi-static problem is solved, see [35, 36]. In particular, the geometrical nonlinear problem is solved using the Newton-Raphson method, along with an opportune arc-length path-following constraint. More detail about the arc-length method adopted can be found in the works by Crisfield [44, 45] and Carrera [46].
- For each equilibrium state of interest, the tangent stiffness matrix is calculated, see Fig. 1.
- Here, Eq. (19) is expanded versus the indexes τ and s (theory approximation order) and i and j (shape function) to give:

$$\left(\mathbf{K}_T - \omega^2 \mathbf{M}\right)\, \delta\mathbf{q} = 0 \tag{20}$$

- Natural frequencies and normal modes of the structure subjected to pre-stress states are found by solving the following equation:

$$det\left(\mathbf{K}_T - \omega^2 \mathbf{M}\right) = 0 \tag{21}$$

- Note that natural frequencies and mode shapes of the resting structure ($\mathbf{q} = 0$) are obtained by linearizing the system in hand around the trivial solution to give:

$$det\left(\mathbf{K}_0 - \omega^2 \mathbf{M}\right) = 0 \tag{22}$$

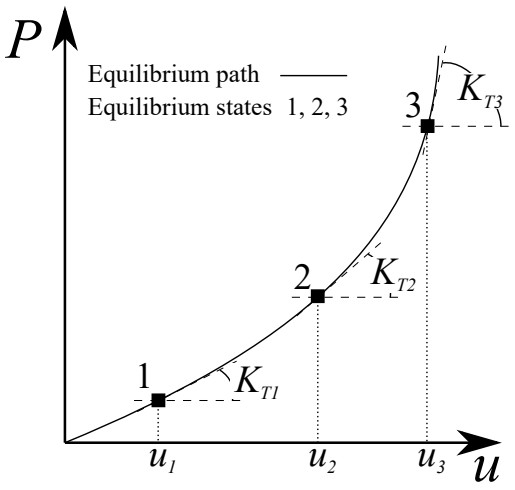

Figure 1: $\mathbf{K}_T$ at the equilibrium conditions of a nonlinear equilibrium path.

4 Numerical results

In this section, we demonstrate how natural frequencies of composite structures are affected by large displacements/rotations and pre-stress states. Quasi-static nonlinear analyses of symmetric and asymmetric laminated beams subjected to various boundary conditions and loadings were carried out first. Linearized vibrations were thus performed to show important mode aberration and to highlight the high efficacy of the proposed model.

4.1 Vibration of asymmetric beam subjected to large bending displacement

A cantilever beam undergoing large deflection due to a uniform transverse pressure was considered in the first analysis case. The beam is composed by two layers of an orthotropic material with Young moduli $E_1 = 144.8$ GPa, $E_2 = E_3 = 9.65$ GPa, Poisson's ratios $\nu_{12} = \nu_{13} = \nu_{23} = 0.3$ and shear moduli $G_{12} = G_{13} = 3.45$ GPa and $G_{23} = 4.14$ GPa. Figure 2 shows the loading condition of the proposed analysis case, along with the cross-section of the beam and the stacking sequence, which is [90°/0°]. The ratio between the thickness and the width of the cross-section t/w is equal to 0.6, and the length-to-side ratio L/w is 9. For all the subsequent analyzed cases, 10 B4 elements and a layerwise approximation employing one L9 discretization per layer were used in the context of CUF. The nonlinear static behavior of this beam model was already validated in [36]. Figure 3 reports the quasi-static equilibrium

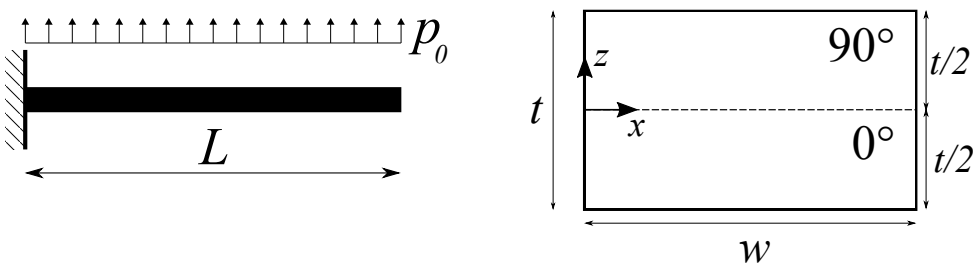

Figure 2: Loading condition and cross-section geometry of the asymmetric cross-ply beam.

curve for the analyzed beam. The solution is achieved using an arc-length method, and the

deformed configurations of some nonlinear condition are depicted.

The natural frequencies of the nonlinear analysis are calculated next. At each step of the

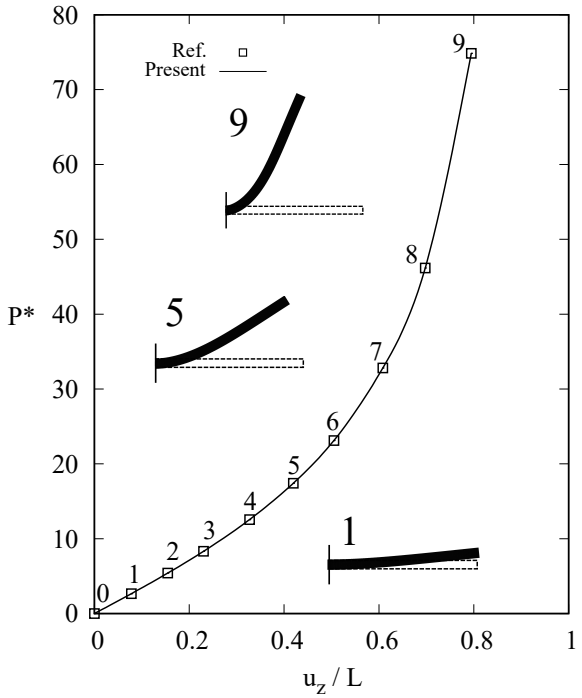

Figure 3: Equilibrium curve of the asymmetric cross-ply beam subjected to vertical pressure. $p^* = \dfrac{p_0\, L^4}{E_2\, h^4}$. Reference results from Pagani and Carrera [36].

equilibrium path, free vibrations are evaluated making use of the local tangent stiffness of the deformed configuration. Table 1 shows the values of the natural frequencies for two bending and one torsional modal shapes. The values of u_z/L are referred to Fig. 3. It can be noticed that the first natural frequency increases as the load rises. By contrast, the natural frequencies of the second bending modal shape decreases until u_z/L equals to 0.608, and then it increases, reaching the value of 12.72 at the end of the equilibrium path. The two bending mode shapes in the table correspond to the first two natural frequencies, whose trends are reported in Fig. 4 along with those of the 3rd, 4th, and 5th natural frequencies. Also, Table 1 demonstrates that the torsional natural frequency increases for higher pre-stresses and exhibits oscillations in high displacement ranges. For the sake of completeness, the trends of the the natural frequencies from the 6th to the 10th are shown in Fig. 5. Curve 8 corresponds to the natural frequency of the torsional modal shape. In Fig. 5, the attention is focussed on the distribution of the 7th, 8th and 9th natural frequencies, between $f = 120Hz$ and $f = 160Hz$. Here, we underline the crossing between mode 7 and mode 8 (second torsion) and the interaction with mode 9. Also, Fig. 6 shows the evolution of these modes all along the quasi static equilibrium path of the structure.

4.2 Vibration of symmetric laminated beam-column

The post-buckling behaviour of a symmmetric cross-ply slender beam is addressed hereafter. The loading and boundary conditions are reported in Fig. 7. The analyzed beam is simply supported and undergoes an axial compression load. Due to the geometric and material symmetry, a small load d is necessary to be applied to enforce the unstable solution branches,

	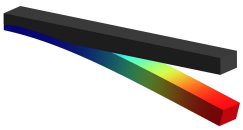	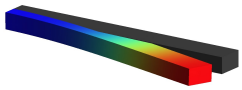	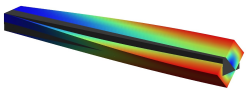
u_z/L	f_1	f_2	f_4
0.000	5.77	14.11	41.20
0.078	5.81	14.03	41.88
0.155	5.89	13.74	43.03
0.230	6.24	13.44	45.40
0.327	6.22	12.74	46.43
0.419	6.52	12.24	48.27
0.505	7.42	12.21	51.85
0.608	7.53	11.69	51.50
0.698	9.31	12.54	56.66
0.795	9.85	12.72	54.48

Table 1: Natural frequencies (Hz) of the bending modes and torsional mode at various steps of the nonlinear analysis. Cantilever asymmetric beam subjected to transverse pressure case.

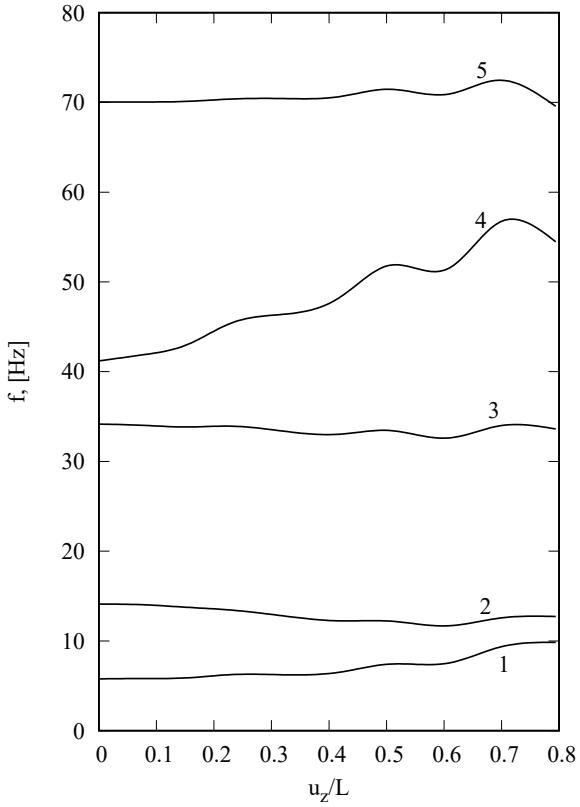

Figure 4: Natural frequencies (Hz) from 1st mode to 5th mode. Cantilever asymmetric beam subjected to transverse pressure case.

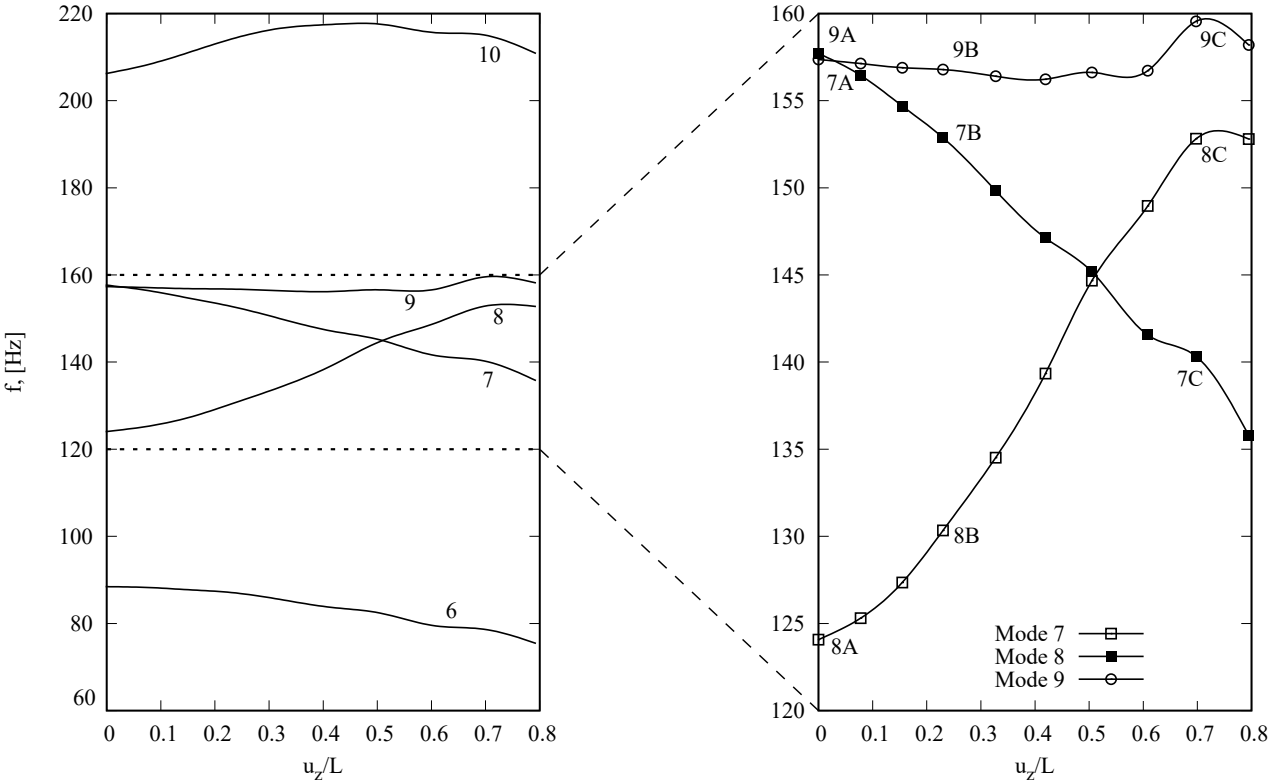

Figure 5: Frequency aberration from 6th mode to 10th mode for the cantilever cross-ply beam subjected to bending pressure with particular attention given to the 120 Hz and 160 Hz range.

as depicted in the figure. d is applied at the middle cross-section of the beam and along the transverse direction. The beam is made of three layers of an orthotropic material with Young moduli $E_1 = 155.0$ GPa, $E_2 = E_3 = 15.5$ GPa, Poisson's ratios $\nu_{12} = \nu_{13} = \nu_{23} = 0.25$ and shear moduli $G_{12} = G_{13} = 9.3$ GPa and $G_{23} = 7.75$ GPa. The geometric conditions are reported in Fig. 7, and the length-to-side ratio equals $L/t = 50$, with a square cross-section. The stacking sequence is $[0°/90°/0°]$, and each layer has the same thickness, which is equal to $t/3$.

The post-buckling quasi-static equilibrium curve of the simply-supported beam is reported in Fig. 8, which shows the transverse displacement versus the loading P according to the high-order 3L16 beam model, see Ref. [36]. The displacement is measured at the middle cross-section. Some of the deformed configurations are reported in the same figure. In the next step, at each equilibrium state of the nonlinear analysis, first 10 natural frequencies are calculated. Table 2 reports the natural frequencies of the first two bending and the torsional modal shapes. It can be noticed that the frequency of the first bending mode decreases and almost goes to zero in correspondence of the critical buckling load, and then it increases, as expected. The same behaviour is demonstrated in [47], for the buckling case of a metallic beam. The natural frequency of the second bending mode shape has the same trend, but there is no evidence of this modal shape at higher load values. The same phenomenon happens in the case of the torsional mode, which suddenly drops from the value of 0.16274 Hz at $P^* = 7.921$ to 0.11762 Hz at $P^* = 8.119$.

Figure 9 shows the trend of the first six natural frequencies as a function of the compression load. In detail, Fig. 9(a) demonstrates the first two bending modes (whose frequencies are also reported in Table 2). Figure 9(b) shows the 3rd and the 4th modes, which represent the bending mode in the yz and the yx planes, respectively. The 3rd natural frequency disappears

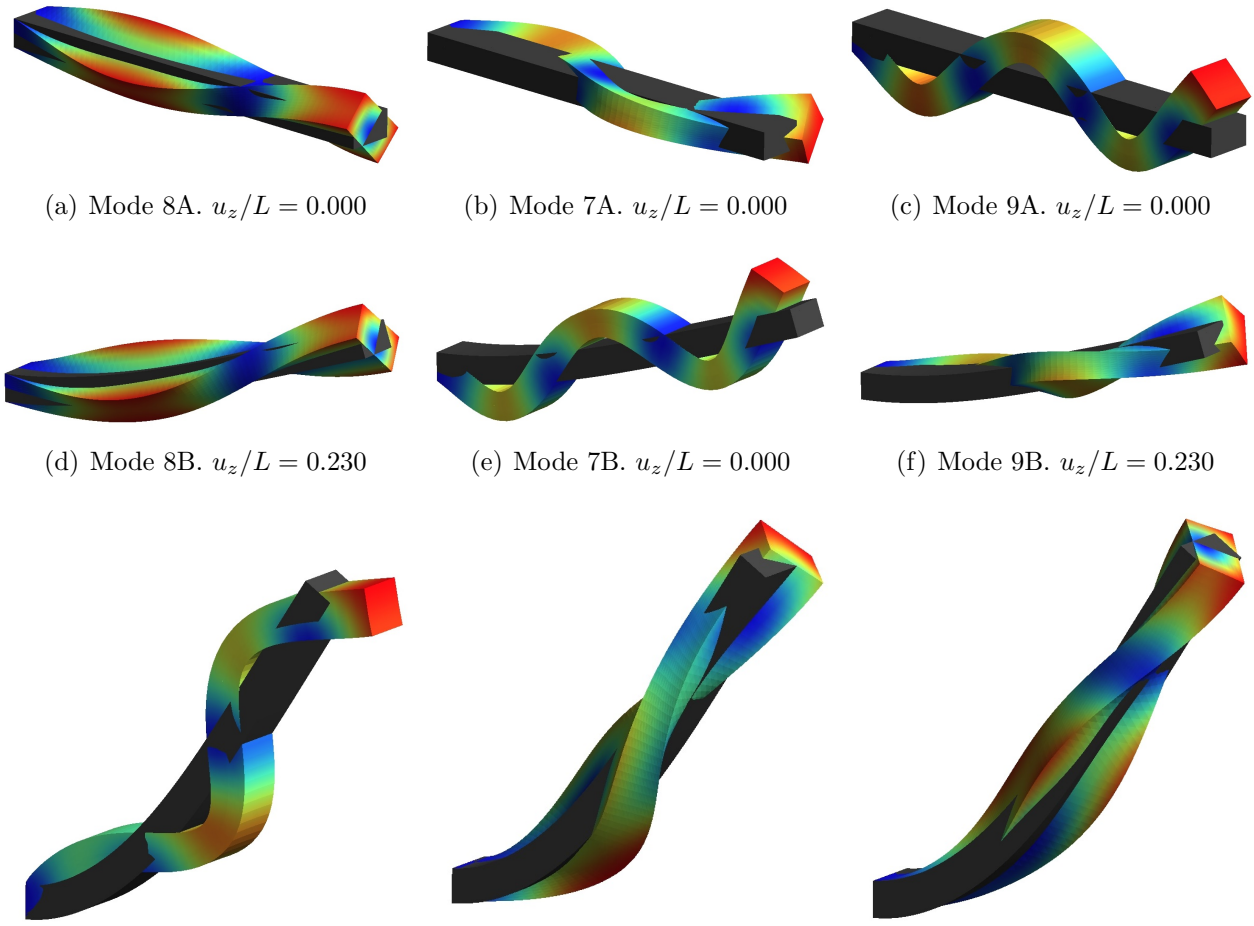

(a) Mode 8A. $u_z/L = 0.000$ (b) Mode 7A. $u_z/L = 0.000$ (c) Mode 9A. $u_z/L = 0.000$

(d) Mode 8B. $u_z/L = 0.230$ (e) Mode 7B. $u_z/L = 0.000$ (f) Mode 9B. $u_z/L = 0.230$

(g) Mode 7C. $u_z/L = 0.698$ (h) Mode 8C. $u_z/L = 0.698$ (i) Mode 9C. $u_z/L = 0.698$

Figure 6: Modal shapes of the 7th, 8th and 9th natural frequencies of the asymmetric cross-ply beam subjected to vertical pressure. Numbers refer to Fig. 5.

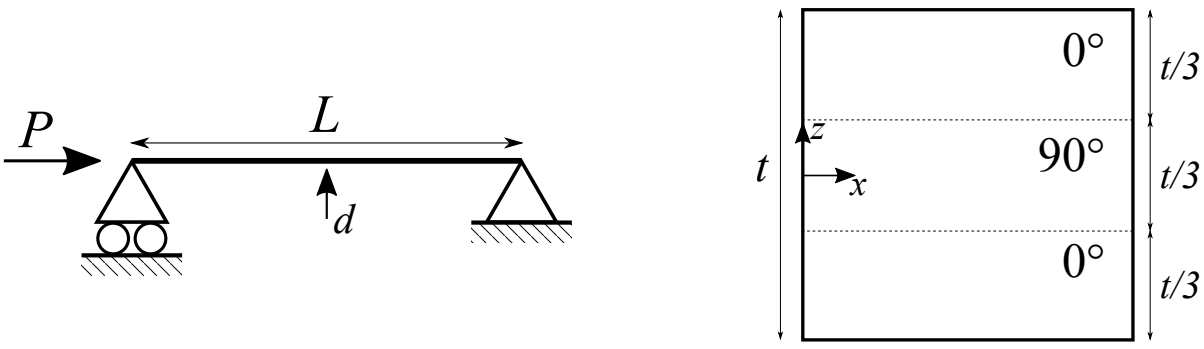

Figure 7: Loading condition and cross-section geometry of the simply-supported symmetric cross-ply beam.

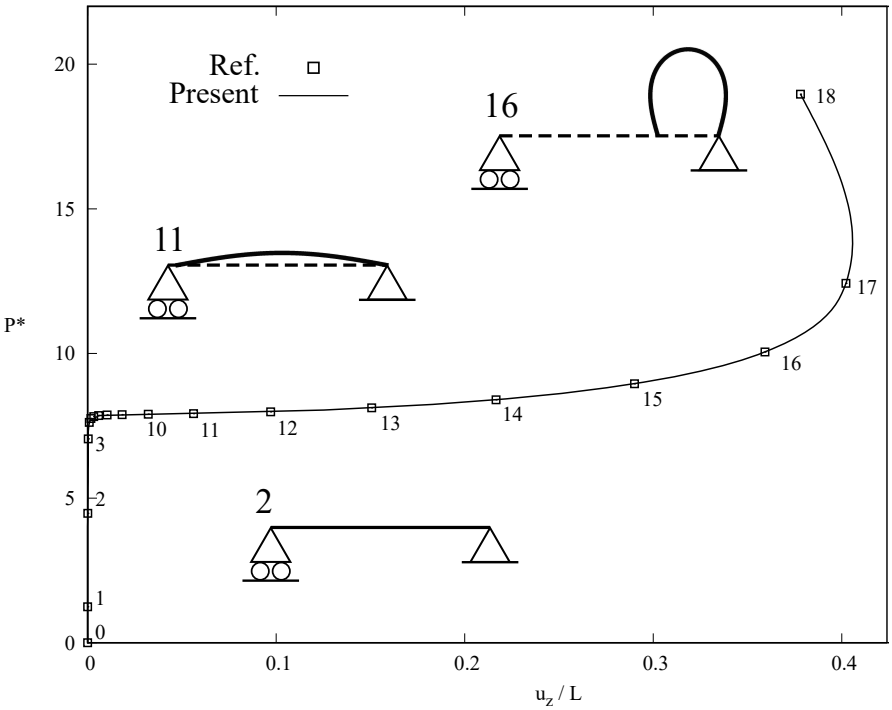

Figure 8: Equilibrium curve of the simply-supported symmetric beam subjected to compression. $P^* = \dfrac{p_0\, L^2}{E_2\, h^4}$. Reference results from Pagani and Carrera [36].

when $P^* = 8.955$, as previously seen for the 2nd mode. The 4th mode, instead, presents an oscillatory behaviour around $P^* = 8.400$. A similar trend is evident for the 5th and 6th modes in Fig. 9(c). Figure 10 reports the mode shapes of the previously reported frequencies in correspondence of the buckling load. Next, Fig. 11 shows the trend of the natural frequencies from the 7th to the 10th. Figure 11(a) reports the trend of the torsional and bending mode. The natural frequency of the torsional mode suddenly drops at $P^* = 8.119$, going below the 6th mode. Finally, Fig. 11(b) shows the changes of two bending frequencies. The correspondent modal shapes are reported in Fig. 12.

4.3 Nonlinear vibration of asymmetric laminated beam-column and comparison with trivial linearized solution

As a final example, asymmetric cross-ply cantilever beam subjected to compression is addressed. The beam is made of two layers with $E_1 = 144.8$ GPa, $E_2 = E_3 = 9.65$ GPa, $\nu_{12} = \nu_{13} = \nu_{23} = 0.3$, $G_{12} = G_{13} = 3.45$ GPa and $G_{23} = 4.14$ GPa. Three different stacking sequences have been analyzed, $[0°/45°]$, $[0°/90°]$ and $[15°/-45°]$. A loading P is applied at the free end as shown in Fig. 13, which also reports the geometric properties, $L/w = 9$, $t/w = 0.6$. The two layers have the same thickness $t/2$. One L16 Lagrange polynomial is employed to approximate the kinematics of each layer on the cross-section in a layerwise sense and, on the other hand, 10 B4 are used along the beam axis. Fig 14 shows the nonlinear trend of the z-coordinate displacement of the free end for each stacking sequence and for different compression states. This static response was validated in [36]. As for the previous analysis cases, at each equilibrium step of the quasi-static response, the linearized eigenvalue problem is solved by accounting for the tangent stiffness, and the trend of the natural frequencies is investigated.

		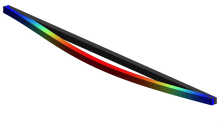	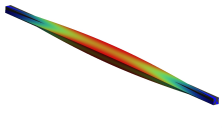
P^*	f_1	f_2	f_7
0.00	0.01400	0.01611	0.16930
1.243	0.01285	0.01503	0.16916
4.473	0.00922	0.01187	0.16891
7.045	0.00454	0.00847	0.16870
7.618	0.00138	0.00719	0.16862
7.885	0.00070	0.00703	0.16802
7.921	0.00124	0.00664	0.16274
8.119	0.00309	–	0.11762
8.955	0.00557	0.01184	–
12.43	0.00829	–	–

Table 2: Natural frequencies (Hz) of bending modes and torsional mode at various steps of the nonlinear analysis. Simply-supported symmetric beam subjected to compression case. $P^* = \dfrac{P\,L^2}{b\,h^3\,E_2}$.

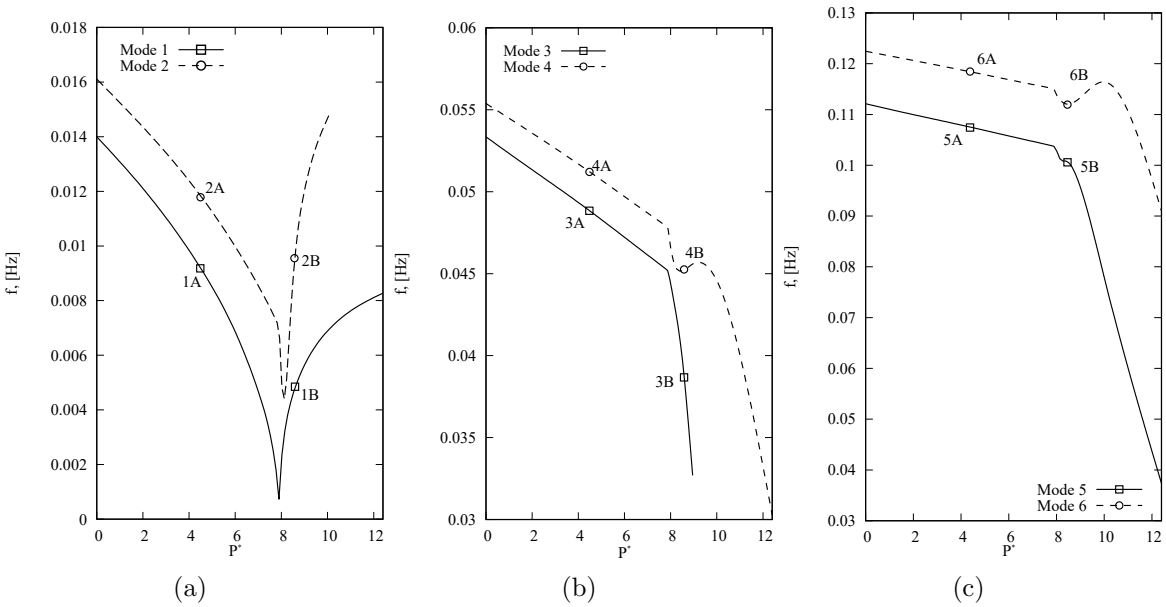

(a) (b) (c)

Figure 9: Natural frequency trends of the first 6 modes for the simply-supported symmetric beam subjected to compression. $P^* = \dfrac{P\,L^2}{b\,h^3\,E_2}$.

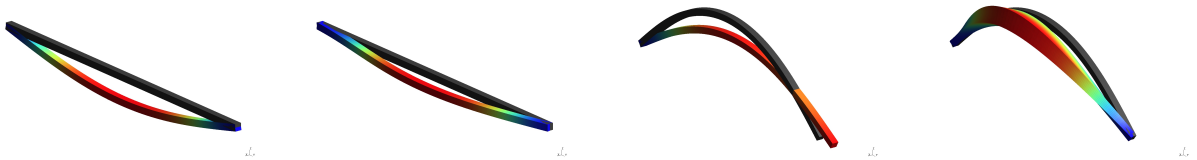

(a) Mode 1A. $P^* = 4.473$ (b) Mode 2A. $P^* = 4.473$ (c) Mode 1B. $P^* = 8.400$ (d) Mode 2B. $P^* = 8.400$

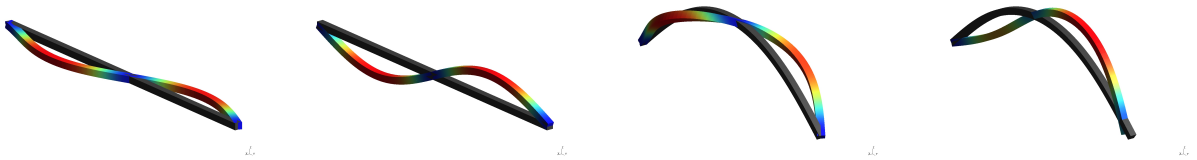

(e) Mode 3A. $P^* = 4.473$ (f) Mode 4A. $P^* = 4.473$ (g) Mode 3B. $P^* = 8.400$ (h) Mode 4B. $P^* = 8.400$

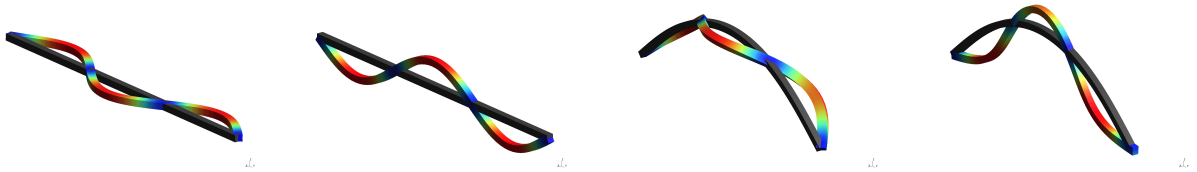

(i) Mode 5A. $P^* = 4.473$ (j) Mode 6A. $P^* = 4.473$ (k) Mode 5B. $P^* = 8.400$ (l) Mode 6B. $P^* = 8.400$

Figure 10: Modal shapes of the of the first 6 modes for the simply-supported symmetric beam subjected to compression. Numbers refer to Fig 9. $P^* = \dfrac{P\,L^2}{b\,h^3\,E_2}$.

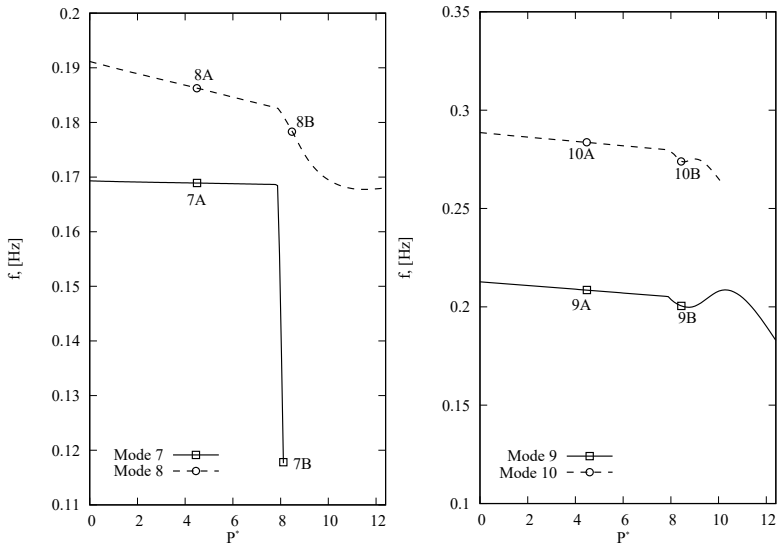

(a) (b)

Figure 11: Natural frequency trends of the 7th, 8th (a), 9th and 10th (b) modes for the simply-supported symmetric beam subjected to compression. $P^* = \dfrac{P\,L^2}{b\,h^3\,E_2}$.

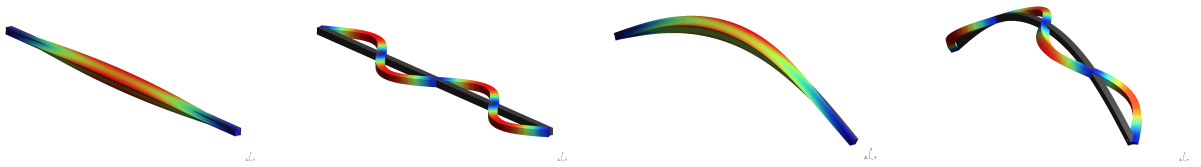

(a) Mode 7A. $P^* = 4.473$ (b) Mode 8A. $P^* = 4.473$ (c) Mode 7B. $P^* = 8.119$ (d) Mode 8B. $P^* = 8.400$

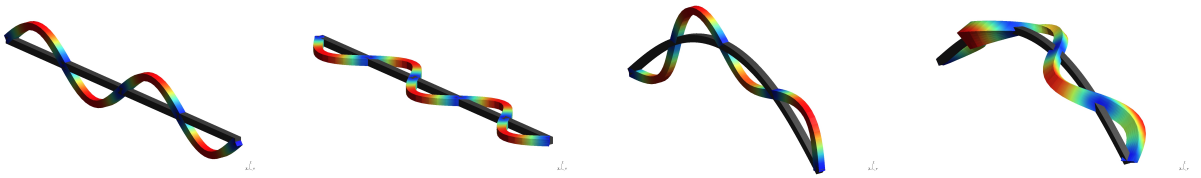

(e) Mode 9A. $P^* = 4.473$ (f) Mode 10A. $P^* = 4.473$ (g) Mode 9B. $P^* = 8.400$ (h) Mode 10B. $P^* = 8.400$

Figure 12: Modal shapes of the 7th, 8th, 9th and 10th modes for the simply-supported symmetric beam subjected to compression. Numbers refer to Fig 9. $P^* = \dfrac{P\,L^2}{b\,h^3\,E_2}$.

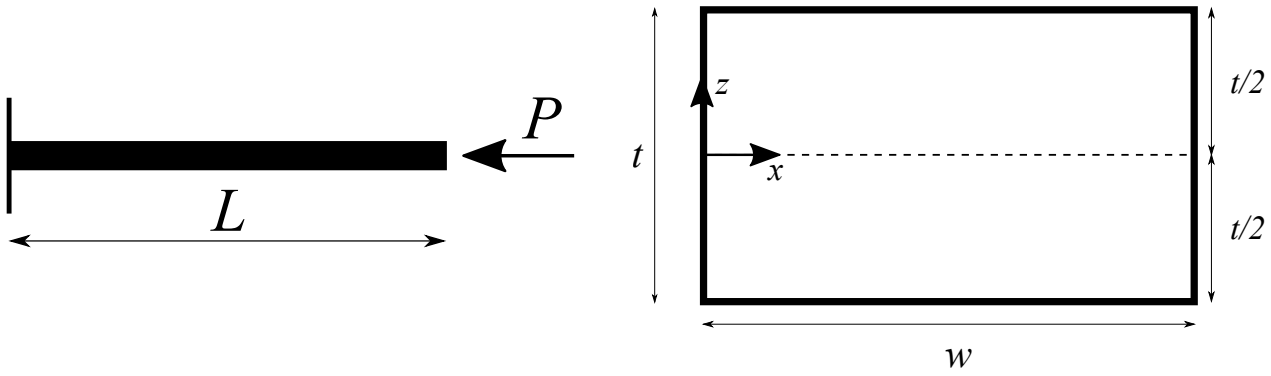

Figure 13: Loading condition and cross-section geometry for the cantilever asymmetric cross-ply beam subjected to compression.

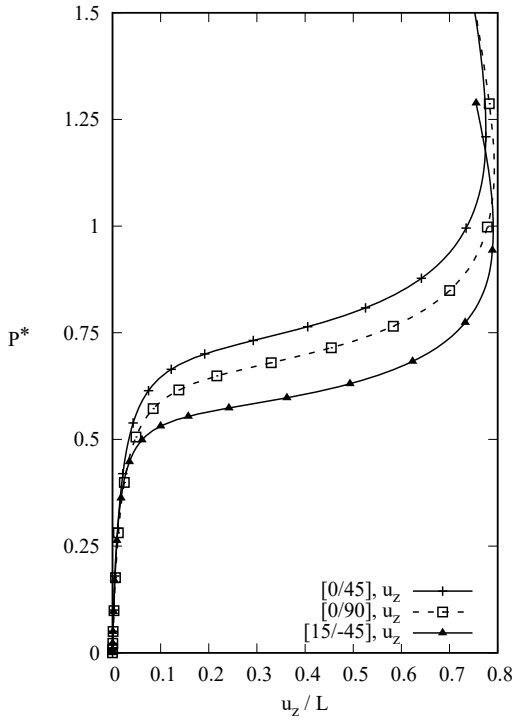

Figure 14: Equilibrium curve of the cantilever asymmetric cross-ply beam subjected to compression. $P^* = \dfrac{P\,L^2}{E_2\,b\,h^3}$.

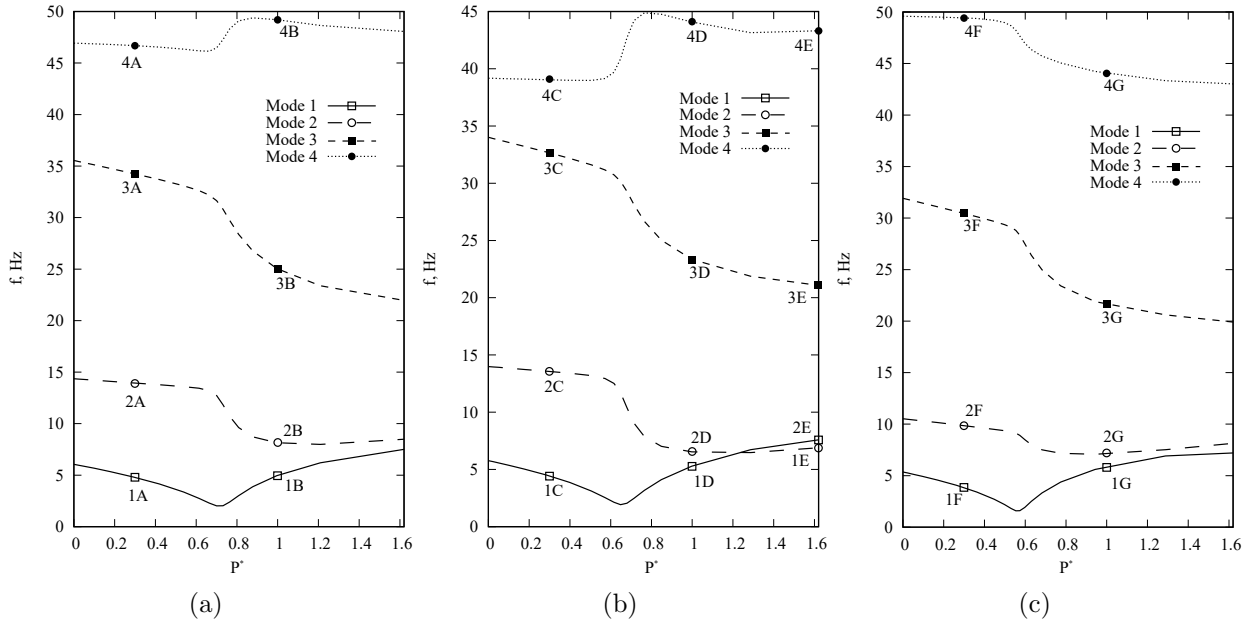

Figure 15: Natural frequency trends of the first 4 modes for the cantilever asymmetric cross-ply beam subjected to compression. (a) [0°/45°], (b) [0°/90°], (c) [15°/−45°]. $P^* = \dfrac{P\,L^2}{E_2\,b\,h^3}$.

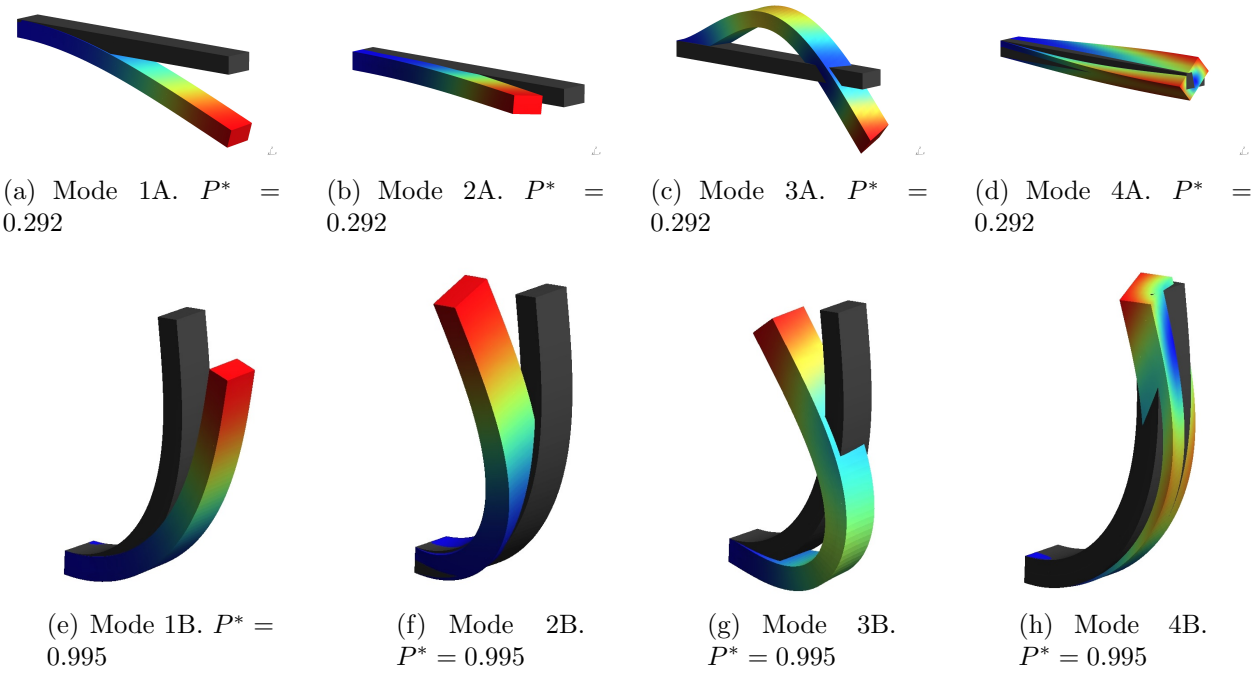

(a) Mode 1A. $P^* = 0.292$ (b) Mode 2A. $P^* = 0.292$ (c) Mode 3A. $P^* = 0.292$ (d) Mode 4A. $P^* = 0.292$

(e) Mode 1B. $P^* = 0.995$ (f) Mode 2B. $P^* = 0.995$ (g) Mode 3B. $P^* = 0.995$ (h) Mode 4B. $P^* = 0.995$

Figure 16: Modal shapes of the first 4 modes for the cantilever asymmetric cross-ply beam subjected to compression. Numbers refer to Fig. 15(a). $P^* = \dfrac{P\,L^2}{E_2\,b\,h^3}$.

Figures 15 shows the distribution of the natural frequencies of four modes for the $[0°/45°]$, $[0°/90°]$ and $[15°/-45°]$ stacking sequences, respectively. Moreover, Figures 16, 17 and 18 show the modal shapes of the 4 modes, for $P^* = 0.3$ and $P^* = 1$. Clearly, the modal shapes are the same for the three lamination cases. In detail, the 1st and the 2nd modes are the bending in the yz and yx plane respectively, the 3rd is a bending mode and the 4th is the torsional mode. The interesting aspect of this analysis arises from the study of the distribution of the first two natural frequencies of the $[0°/90°]$ stacking sequence case (see Fig. 15(b)). In fact, around $P^* = 1.250$, a crossing phenomenon between the two natural frequencies appears. This is also demonstrated by Figure 18, where the modal shape at $P^* = 1.630$ is further depicted, to show the aberration between the 1st and the 2nd modes.

Finally, an analysis of the difference between linearized frequencies evaluated around trivial states and linearized frequencies calculated around nonlinear equilibrium states is proposed. Figure 19 shows the trend of the linearized and nonlinear frequencies associated at the first two modes for the three stacking sequences previously analysed. It can be pointed out that the first natural frequencies (that is associated to the bending mode in the yz plane) disappear when the buckling-like phenomenon occurs within the structure. For the second mode, the frequency evaluated around the trivial state is always higher than the nonlinear one, except for the $[15°/-45°]$ stacking sequence case, where it becomes lower after P^* reaches the value of 1.3. Also, it is clear that crossing and veering phenomena are completely unforeseen by the trivial linearized model. Moreover, for the $[0°/45°]$, the linear and nonlinear distribution of the axial and transverse component of the stress tensor are reported in Figs. 20 and 21. Clearly, for the σ_{yy} component, the trend is similar for both analyses, but for the nonlinear cases the stress reaches higher values. Instead, for the σ_{yz} component, the trend between the two analyses is different, and the L16 Lagrange polynomial along with the layerwise approach can catch the parabolic trend of the stress for the nonlinear case. As for the σ_{yy}, also the σ_{yz}

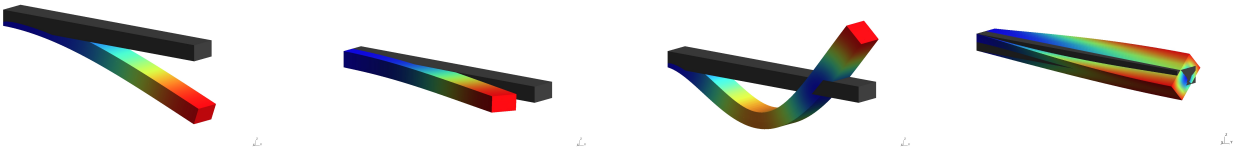

(a) Mode 1C. $P^* = 0.292$ (b) Mode 2C. $P^* = 0.292$ (c) Mode 3C. $P^* = 0.292$ (d) Mode 4C. $P^* = 0.292$

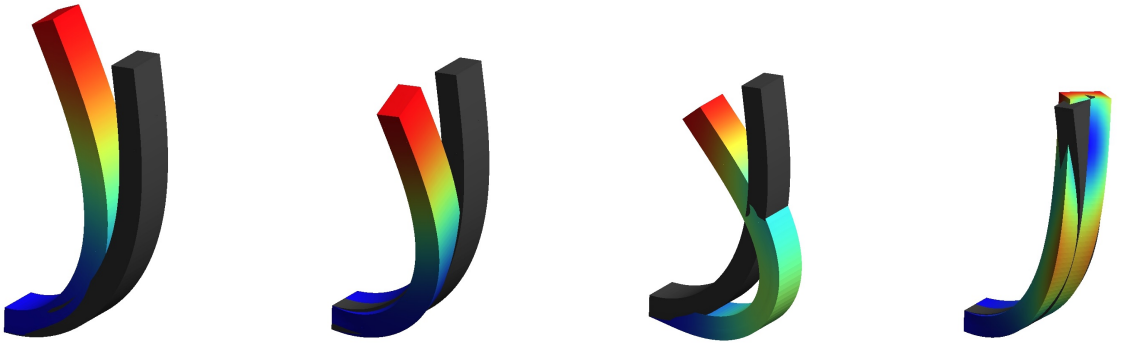

(e) Mode 1D. $P^* = 0.995$ (f) Mode 2D. $P^* = 0.995$ (g) Mode 3D. $P^* = 0.995$ (h) Mode 4D. $P^* = 0.995$

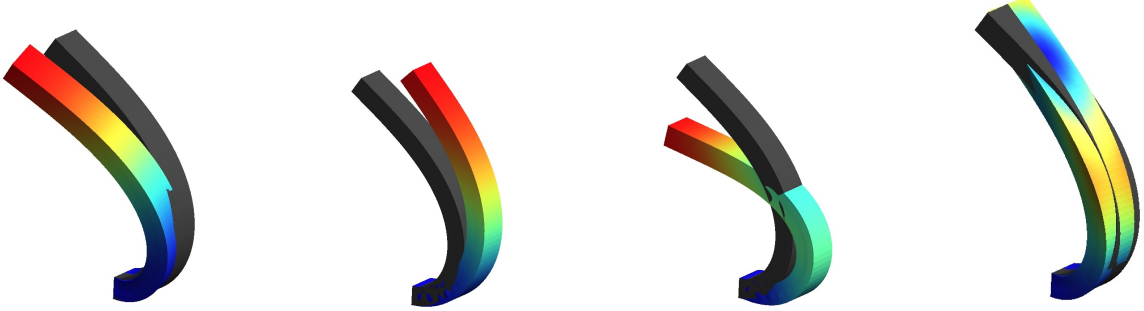

(i) Mode 1E $P^* = 1.630$ (j) Mode 2E. $P^* = 1.630$ (k) Mode 3E. $P^* = 1.630$ (l) Mode 4E. $P^* = 1.630$

Figure 17: Modal shapes of the first 4 modes for the cantilever asymmetric cross-ply beam subjected to compression. Numbers refer to Fig. 15(b). $P^* = \dfrac{P\,L^2}{E_2\,b\,h^3}$.

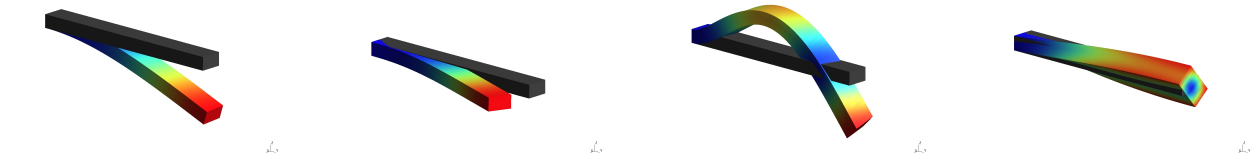

(a) Mode 1F. $P^* = 0.292$ (b) Mode 2F. $P^* = 0.292$ (c) Mode 3F. $P^* = 0.292$ (d) Mode 4F. $P^* = 0.292$

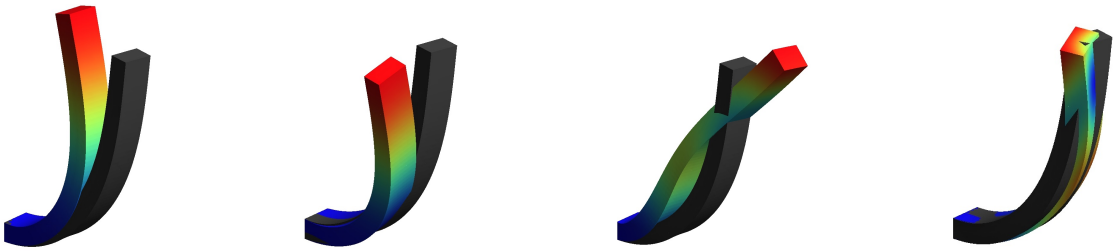

(e) Mode 1G. $P^* = 0.995$ (f) Mode 2G. $P^* = 0.995$ (g) Mode 3G. $P^* = 0.995$ (h) Mode 4G. $P^* = 0.995$

Figure 18: Modal shapes of the first 4 modes for the cantilever asymmetric cross-ply beam subjected to compression. Numbers refer to Fig. 15(c). $P^* = \dfrac{P\,L^2}{E_2\,b\,h^3}$.

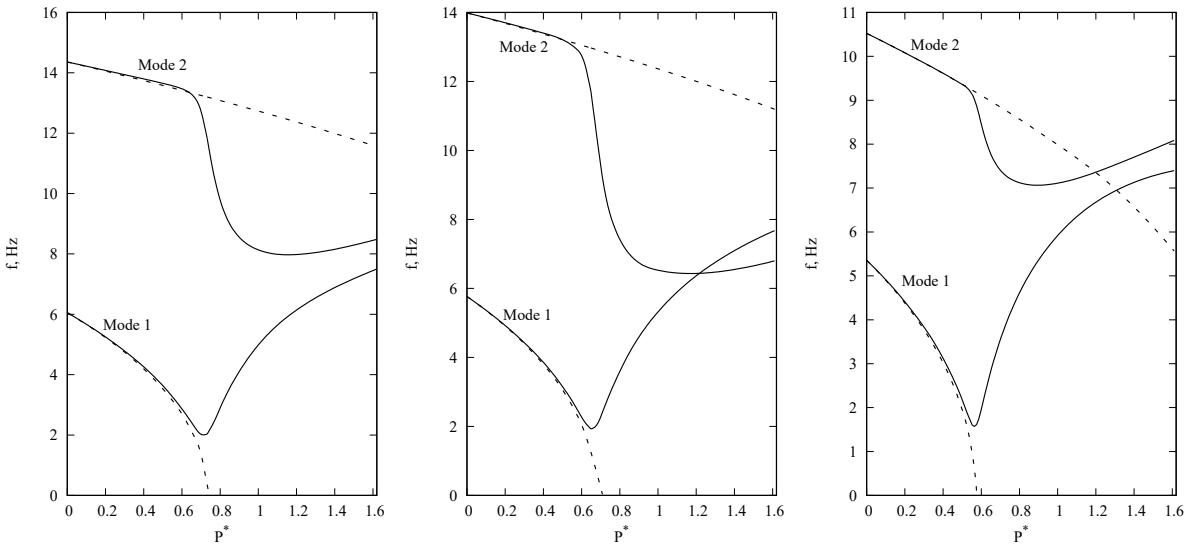

(a) (b) (c)

Figure 19: Linearized frequency around nonlinear equilibrium states (continuous line) and linearized frequency around trivial state (dashed line) of the 1st and 2nd frequency for the cantilever asymmetric cross-ply beam subjected to compression. (a) [0°/45°], (b) [0°/90°], (c) [15°/−45°]. $P^* = \dfrac{P\,L^2}{E_2\,b\,h^3}$.

has higher values for the nonlinear case, as expected.

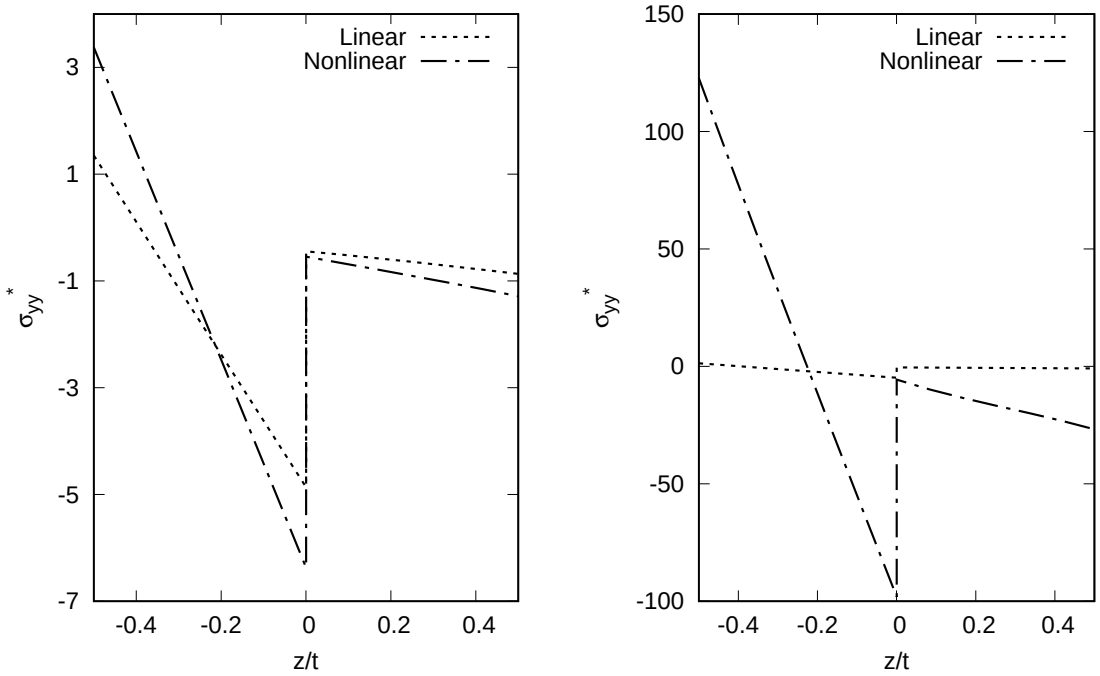

Figure 20: Through the thickness distribution of axial stress component according to linear and full geometric nonlinear analyses for $P^* = 0.3$ (a) and $P^* = 1$ (b). The stacking sequence is $[0°/45°]$. $\sigma^*_{yy} = \dfrac{\sigma_{yy}\, h^2}{P}$. Cantilever asymmetric cross-ply beam subjected to compression case.

5 Conclusions

The present research paper has demonstrated that composite structures can be subjected to severe frequency changes and modes aberration as a consequence of geometrical nonlinear equilibrium states. For this purpose, we have used the Carrera Unified Formulation (CUF), which, when combined to variational principles and finite element approach, generates a unique framework for the implementation of low- to high-fidelity models for composite structures, including eventually layerwise kinematics. A path-following method is used to solve the nonlinear quasi-static problem of composite beams subjected to mechanical loadings, whereas the evaluation of the dynamic properties demands for the linearization of the equations of motion at each equilibrium state of the whole equilibrium path. It is demonstrated that the most critical change of the modal shapes occurs in the case of structure subjected to compression load. In the post-buckling regime, in fact, some modes fade and others show an oscillatory behaviour (bending modes) or a sudden drop of the natural frequency associated (torsional mode). Finally, a crossing phenomenon between the first two modes appears in the post-buckling regime of a cross-ply beam with cross-ply lamination $[0°/90°]$. In contrast, the other stacking sequences analyzed ($[0°/45°]$ and $[15°/-45°]$) do not show such a behaviour, which demonstrate that dynamics aberrations can be tailored with the use of composite materials.

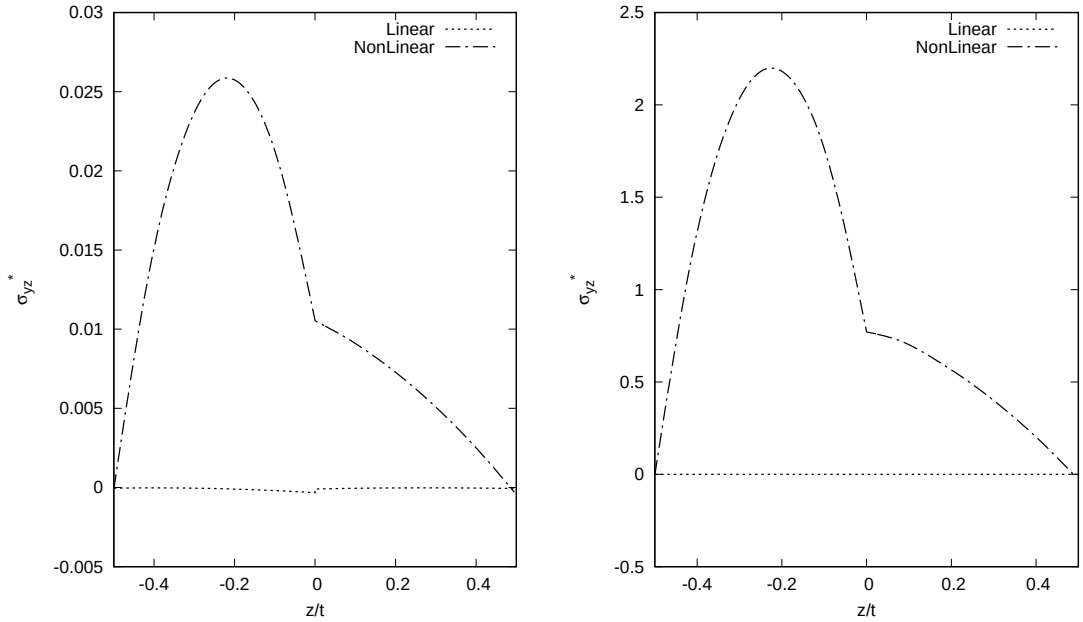

Figure 21: Linear and nonlinear distribution of σ_{yz} along the thickness for (a) $P^* = 0.3$ and (b) $P^* = 1$ for the $[0°/45°]$ stacking sequence. $\sigma^*_{yz} = \dfrac{\sigma_{yz}\, h^2}{P}$. Cantilever asymmetric cross-ply beam subjected to compression case.

References

[1] M.A. Biot. Non-linear theory of elasticity and the linearized case for a body under initial stress. *The London, Edinburgh, and Dublin Philosophical Magazine and Journal of Science*, 27(183):468–489, 1939.

[2] S.D. Akbarov. Recent investigations on dynamic problems for an elastic body with initial (residual) stresses. *International Applied Mechanics*, 43(12):1305, 2007.

[3] S.D. Akbarov and M. Ozisik. Dynamic interaction of a prestressed nonlinear elastic layer and a half-plane. *International Applied Mechanics*, 40(9):1056–1063, 2004.

[4] R.W. Ogden and D.G. Roxburgh. The effect of pre-stress on the vibration and stability of elastic plates. *International Journal of Engineering Science*, 31(12):1611–1639, 1993.

[5] G. Herrmann. The influence of initial stress on the dynamic behavior of elastic and viscoelastic plates. *Publications of the International Association for Bridge and Structural Engineering*, 16:275–294, 1956.

[6] C.T. Sun and J.M. Whitney. Dynamic response of laminated composite plates under initial stress. *AIAA Journal*, 14(2):268–270, 1976.

[7] L.N. Virgin. *Vibration of axially-loaded structures*. Cambridge University Press, Cambridge, UK., 2007.

[8] S.P. Timoshenko. On the transverse vibrations of bars of uniform cross section. *Philosophical Magazine*, 43:125–131, 1922.

[9] L.-Li. Ke, J. Yang, and S. Kitipornchai. Nonlinear free vibration of functionally graded carbon nanotube-reinforced composite beams. *Composite Structures*, 92(3):676–683, 2010.

[10] P. Zhu, Z.X. Lei, and K.M. Liew. Static and free vibration analyses of carbon nanotube-reinforced composite plates using finite element method with first order shear deformation plate theory. *Composite Structures*, 94(4):1450–1460, 2012.

[11] A.W. Leissa. The free vibration of rectangular plates. *Journal of Sound and Vibration*, 31(3):257–293, 1973.

[12] A.W. Leissa. *Vibration of shells*. Scientific and Technical Information Office, National Aeronautics and Space Administration Washington, 1973.

[13] A.W. Leissa and M.S. Qatu. *Vibrations of Continuous Systems.* McGraw-Hill, 2011.

[14] D.H. Hodges, A.R. Atilgan, M.V. Fulton, and L.W. Rehfield. Free-vibration analysis of composite beams. *Journal of the American Helicopter Society*, 36(3):36–47, 1991.

[15] K. Chandrashekhara, K. Krishnamurthy, and S. Roy. Free vibration of composite beams including rotary inertia and shear deformation. *Composite Structures*, 14(4):269–279, 1990.

[16] K. Chandrashekhara and K.M. Bangera. Free vibration of composite beams using a refined shear flexible beam element. *Computers & structures*, 43(4):719–727, 1992.

[17] O. Song and L. Librescu. Free vibration of anisotropic composite thin-walled beams of closed cross-section contour. *Journal of Sound and Vibration*, 167(1):129–147, 1993.

[18] J. Lee. Free vibration analysis of delaminated composite beams. *Computers & Structures*, 74(2):121–129, 2000.

[19] T. Kant and K. Swaminathan. Analytical solutions for free vibration of laminated composite and sandwich plates based on a higher-order refined theory. *Composite structures*, 53(1):73–85, 2001.

[20] A.K. Noor and W.S. Burton. Stress and free vibration analyses of multilayered composite plates. *Composite Structures*, 11(3):183–204, 1989.

[21] R.K. Kapania and S. Raciti. Recent advances in analysis of laminated beams and plates, Part I: Shear effects and buckling. *AIAA Journal*, 27(7):923–935, 1989.

[22] R.K. Kapania and S. Raciti. Recent advances in analysis of laminated beams and plates, Part II: Vibrations and wave propagation. *AIAA Journal*, 27(7):935–946, 1989.

[23] Y.X. Zhang and C.H. Yang. Recent developments in finite element analysis for laminated composite plates. *Composite Structures*, 88(1):147–157, 2009.

[24] J.N. Reddy. A generalization of two-dimensional theories of laminated composite plates. *Communications in applied numerical methods*, 3(3):173–180, 1987.

[25] D.H. Hodges. *Nonlinear composite beam theory.* American Institute of Aeronautics and Astronautics, 2006.

[26] C.-Y. Chia. Geometrically nonlinear behavior of composite plates: A review. *Applied Mechanics Reviews*, 41(12):439–451, 1988.

[27] Y.X. Zhang and K.S. Kim. Geometrically nonlinear analysis of laminated composite plates by two new displacement-based quadrilateral plate elements. *Composite Structures*, 72(3):301–310, 2006.

[28] L.W. Zhang and K.M. Liew. Geometrically nonlinear large deformation analysis of functionally graded carbon nanotube reinforced composite straight-sided quadrilateral plates. *Computer Methods in Applied Mechanics and Engineering*, 295:219–239, 2015.

[29] H. Abramovich, D. Govich, and A. Grunwald. Buckling prediction of panels using the vibration correlation technique. *Progress in Aerospace Sciences*, 78:62–73, 2015.

[30] M.A. Arbelo, K. Kalnins, O. Ozolins, E. Skukis, S.G.P. Castro, and R. Degenhardt. Experimental and numerical estimation of buckling load on unstiffened cylindrical shells using a vibration correlation technique. *Thin-Walled Structures*, 94:273–279, 2015.

[31] E. Carrera, G. Giunta, and M. Petrolo. *Beam Structures: Classical and Advanced Theories*. John Wiley & Sons, 2011.

[32] E. Carrera, M. Cinefra, M. Petrolo, and E. Zappino. *Finite element analysis of structures through unified formulation*. John Wiley & Sons, New York, USA, 2014.

[33] I. Kaleel, M. Petrolo, A. M. Waas, and E. Carrera. Computationally efficient, high-fidelity micromechanics framework using refined 1d models. *Composite Structures*, 181:358–367, 2017.

[34] E. Carrera and A. Pagani. Free vibration analysis of civil engineering structures by component-wise models. *Journal of Sound and Vibration*, 333(19):4597–4620, 2014.

[35] A. Pagani and E. Carrera. Unified formulation of geometrically nonlinear refined beam theories. *Mechanics of Advanced Materials and Structures*, 25(1):15–31, 2018.

[36] A. Pagani and E. Carrera. Large-deflection and post-buckling analyses of laminated composite beams by carrera unified formulation. *Composite Structures*, 170:40–52, 2017.

[37] M. Cinefra, M. Petrolo, G. Li, and E. Carrera. Hygrothermal analysis of multilayered composite plates by variable kinematic finite elements. *Journal of Thermal Stresses*, 40(12):1502–1522, 2017.

[38] F. Miglioretti and E. Carrera. Application of a refined multi-field beam model for the analysis of complex configurations. *Mechanics of Advanced Materials and Structures*, 22(1-2):52–66, 2015.

[39] M.A. Crisfield. *Non-linear finite element analysis of solids and structures*. John Wiley & Sons, 1993.

[40] E. Carrera and M. Petrolo. Refined one-dimensional formulations for laminated structure analysis. *AIAA journal*, 50(1):176–189, 2012.

[41] E. Carrera and M. Petrolo. Refined beam elements with only displacement variables and plate/shell capabilities. *Meccanica*, 47(3):537–556, 2012.

[42] K.-J. Bathe. *Finite element procedures*. Klaus-Jurgen Bathe, 2006.

[43] O.C. Zienkiewicz and R. L. Taylor. *The Finite Element Method for Solid and Structural Mechanics*. Elsevier, Amsterdam, Netherlands, 2005.

[44] M.A. Crisfield. A fast incremental/iterative solution procedure that handles "snap-through". In *Computational Methods in Nonlinear Structural and Solid Mechanics*. Elsevier, Amsterdam, Netherlands, 1981.

[45] M.A. Crisfield. An arc-length method including line searches and accelerations. *International journal for numerical methods in engineering*, 19(9):1269–1289, 1983.

[46] E. Carrera. A study on arc-length-type methods and their operation failures illustrated by a simple model. *Computers & structures*, 50(2):217–229, 1994.

[47] A. Pagani, R. Augello, and E. Carrera. Frequency and mode change in the large deflection and post-buckling of compact and thin-walled beams. *Journal of Sound and Vibration*, 432:88–104, 2018.